Magn Reson Mater Phy (2012) 25:381–389
DOI 10.1007/s10334-012-0310-2

RESEARCH ARTICLE

Hepatic lipid composition differs between ob/ob and ob/+ control mice as determined by using in vivo localized proton magnetic resonance spectroscopy

Qiong Ye · Carsten Friedrich Danzer · Alexander Fuchs · Christian Wolfrum · Markus Rudin

Received: 20 October 2011 / Revised: 24 February 2012 / Accepted: 24 February 2012 / Published online: 23 March 2012

Abstract
Object Hepatic lipid accumulation is associated with nonalcoholic fatty liver disease, and the metabolic syndrome constitutes an increasing medical problem. In vivo proton magnetic resonance spectroscopy (^{1}H MRS) allows the assessment of hepatic lipid levels noninvasively and also yields information on the fat composition due to its high spectral resolution.
Materials and methods We applied ^{1}H MRS at 9.4T to study lipid content and composition in eight leptin-deficient ob/ob mice as a model of obesity and in four lean ob/+ control mice at 24 weeks of age. PRESS sequence was used. For accurate estimation of signal intensity, differences in relaxation behavior of individual signals were accounted for each mouse individually. Also, in order to minimize spectral degrading due to motion artifacts, respiration gating was applied.
Results Significant differences between ob/ob and ob/+ control mice were found in both lipid content and composition. The mean chain length was found to be significantly longer in ob/ob mice with a higher fraction of monounsaturated lipids.
Conclusion ^{1}H MRS enables accurate assessment in hepatic lipids in mice, which is attractive for mechanistic studies of altered metabolism given the large number of genetically engineered mouse models available.

Keywords Hepatic steatosis · Mouse · Obesity · Magnetic resonance spectroscopy (MRS)

Abbreviations

CRLB	The Cramer–Rao lower bound
fMUL	Fraction of monounsaturated lipids
FOV	Field-of-view
fPUL	Fraction of polyunsaturated lipids
fSL	Fraction of saturated lipids
fUL	Fraction of unsaturated lipids
fLM	Fractional lipid mass
MCL	Mean chain length
NA	Number of averages
ob/ob	Lep^{ob}/Lep^{ob}
ob/+	$Lep^{ob}/+$
SL	Saturated lipid component
TG	Triglyceride
UL_{total}	Total unsaturated lipid component

Introduction

Hepatic steatosis, characterized by the accumulation of lipid droplets within hepatocytes, is of increasing prevalence among the population. Lipid accumulation in the liver is associated with nonalcoholic fatty liver disease,

Q. Ye · M. Rudin (✉)
Institute for Biomedical Engineering UZH/ETH, University and ETH Zurich, HIT E22.4, Wolfgang-Pauli-Strasse 27, 8093 Zurich, Switzerland
e-mail: rudin@biomed.ee.ethz.ch

C. F. Danzer
Institute of Cell Biology, ETH Zurich, Zurich, Switzerland

A. Fuchs
Institute for Biomedical Engineering UZH/ETH, University and ETH Zurich, 8093 Zurich, Switzerland

C. Wolfrum
Laboratory of Translational Nutritional Biology, ETH Zurich, Zurich, Switzerland

M. Rudin
Institute of Pharmacology and Toxicology, University of Zurich, Zurich, Switzerland

obesity and/or type 2 diabetes [1–3]. An accurate and preferentially non-invasive method for detection and staging hepatic lipid deposition is important for diagnosis and therapy management.

In the last few decades, many methods have been applied for quantification of lipid composition, including gas chromatography, mass spectrometry, ^{1}H and ^{13}C nuclear magnetic resonance (NMR). Both gas chromatography, considered as the golden standard, and mass spectrometry require tissue samples [4–6]. Magnetic resonance spectroscopy (MRS) is a quantitative technique, and due to its non-invasive nature can facilitate longitudinal studies. Due to the high chemical specificity provided by MRS, detailed information on the lipid composition can be obtained [7–11]. In validation studies using different oil samples, good agreement between the lipid composition as derived from ^{1}H and ^{13}C MRS readouts and results derived from gas chromatography analysis has been obtained [9]. In vitro and in vivo ^{1}H MRS were applied to assess the lipid composition in white adipose tissue, brown adipose tissue, tumor, bone marrow, and subcutaneous fat of humans [7, 10, 12–18] and the in vivo spectroscopic results were compared with data from biopsy samples. Similar ^{1}H MRS has been carried out to assess triacylglycerol and fatty acids in livers in humans and rodents both in vivo and ex vivo [19–26].

The objective of our study was to compare the lipid composition in liver of ob/ob and ob/+ control mice. Ob/ob mice are widely used as model of obesity and type 2 diabetes. They are characterized by leptin deficiency, which leads to increased food intake and reduced energy expenditure; in addition, ob/ob mice display a slightly increased feed efficiency (increased body weight gain for identical caloric intake as compared to ob/+ controls) [3, 22, 27, 28]. This metabolic condition causes a redistribution of fat storage from fat pads to non-adipose tissue such as liver, skeletal muscle, heart and pancreas. This increased uptake and storage of lipids in non-adipose tissues is thought to induce cell damage and apoptosis [29, 30]. For example in liver, which plays a unique role in controlling carbohydrate and lipid homeostasis, impairment of mitochondria has been reported [31]. The resulting liver dysfunction has been shown to correlate not only with the total amount of lipids stored, but also with their composition, in particular with factors such as the chain length and the degree of unsaturation [32, 33]. ^{1}H MRS should provide this information in a non-invasive manner.

Materials and methods

Animals and experimental protocol

Twelve male mice were used: eight ob/ob and four age-matched ob/+ controls (Jackson Lab, Charles River Laboratories, Research Models and Services, Germany GmbH) at 24 weeks of age. Prior to the MR examinations the body weight of the animals was determined (61.7 ± 1.8 g in ob/ob vs. 34.9 ± 1.5 g in ob/+). For MRS studies the mice were initially anesthetized using 3% isoflurane, and anesthesia levels were reduced to 1.5–2.25% in a combination of oxygen-air mixture (1/2.5) during the course of the experiments administered via face mask. The mice were positioned prone on a surface coil with the liver on top of the coil center. For physiological monitoring a ML880 16/30 Powerlab system (AD Instruments, Spechbach, Germany) was used. The body temperature was monitored and controlled with water heating. The respiration signal was monitored as well using a balloon sensor, and used for respiration gating. The mice were housed with free access to standard chow and water. All animal experiments were performed in strict adherence to the Swiss Law for Animal Protection.

MRS experiment

In vivo MRS measurements were performed using a Bruker BioSpec 94/30 (Bruker BioSpin GmbH, Ettlingen, Germany) system equipped with 9.4 T magnet with 30 cm bore diameter. A birdcage volume resonator (70 mm inner diameter) and a surface coil (phased array for ob/ob, single loop surface coil for ob/+, due to differences in body sizes) were used for transmission and signal reception respectively. The gradient system was capable of switching 400 mT/m at a minimal rise time of 80 μs. An IntraGate (Bruker BioSpin GmbH, Ettlingen, Germany) pulse sequence was used for anatomical reference images with a field-of-view (FOV) = 40 × 40 mm^2 (ob/ob) and 30 × 30 mm^2 (ob/+), matrix dimension = 256 × 128, T_R = 1.5 s, T_E = 8 ms, and RARE factor = 8. Respiratory-gating was implemented for motion correction. The volume of interest of the subsequent proton spectroscopy was carefully planned on these images to avoid contributions from obvious blood vessels and subcutaneous fat. Single-voxel localized ^{1}H MR spectra were acquired using the PRESS sequence with additional outer volume suppression with the following parameters: voxel volume 3 × 3 × 3 mm^3, repetition time T_R = 6,000 ms, echo times T_E = 12, 18, 24, 30 ms, band width = 4,006 Hz, number of sampling points = 2,048, acquisition time = 511 ms, number of averages (NA) = 40 (ob/ob) and 100 (ob/+). Due to respiration gating, the actual scan time was longer than the scan time calculated by the system. This deviation was minimized by adjusting the duration of the respiration cycle to around 0.5–1 s. For water suppression the VAPOR sequence was used. An unsuppressed spectrum was recorded within the same voxel with NA = 40 (ob/ob) and NA = 10 (ob/+), yielding the water reference signal. For

correcting the measured signal intensities for T_2 effects, the T_2 relaxation time was derived from measurements with $T_R = 6{,}000$ ms, and different echo times $T_E = 12$, 18, 24, and 30 ms and T_2 relaxation times were determined for individual spectral peaks. This was required for accurate quantification of hepatic lipid composition.

Analysis of MRS data

All spectroscopy data were processed using LCModel (Version 6.2-1Q, Stephen Provencher, Oakville, ON, Canada). Nine lipid signals were identified in our murine liver ^{1}H MRS spectra. Peak assignments were based on published data [20] and are summarized in Table 1 [10, 11, 13, 18], which is included to assist the reader. Prior to quantification, T_2 values for individual resonances were derived by single-exponential fitting of the signal intensities obtained for the different echo times T_{Ei}, $I(T_{Ei}) = I(0) \times \exp(-T_{Ei}/T_2)$ yielding corrected peak intensities $I(0)$ for individual peaks of each mouse, where $I(T_{Ei})$ represents the measured intensity for an echo time T_{Ei}. No correction for T_1, since for a T_R of 6 s all resonances except for water can be assumed to be almost fully relaxed [13, 34]. Lip41 and Lip43 from ob/+ control mice were excluded for further quantification, since the spectral region between 3.6 and 5.0 ppm was cut in LCModel due to the interference of the residual water signal.

From the intensity of the nine lipid signals normalized to the number of protons contributing to the signal and the water signal intensity, a number of parameters were derived:

(a) The lipid mass and the fractional lipid mass (fLM): The main contributors to the ^{1}H MR spectrum are protons of water, mono-, di- and triglycerides, phospholipids and free fatty acid, as well as a small amount of cholesterol and cholesterol ester [12, 20, 35]. Contributions from phospholipids can be neglected due to restricted mobility of these membrane lipids giving rise to broad lines [12]. Hence the lipid mass may be estimated from the weighted sum of all (nine) lipid signals with weighting factors 13 accounting for the mass of a =CH– group (Lip52&53), 14 for –CH_2– (Lip13, Lip16, Lip21, Lip23, Lip28, Lip41, Lip43) and 15 for –CH_3 group (Lip09). We assume one –CH_3 group per lipid molecule. Correspondingly the lipid mass may be estimated as:

$$\begin{aligned}\text{Lipid mass} = {} & \frac{1}{2} \times (\text{Lip13} + \text{Lip16} + \text{Lip21} + \text{Lip23} \\ & + \text{Lip28} + \text{Lip41} + \text{Lip43}) \times 14 \\ & + (\text{Lip52\&53}) \times 13 + \frac{1}{3} \times (\text{Lip09}) \\ & \times 15 + \frac{1}{3} \times (\text{Lip09}) \times 12 \\ & + \frac{2}{3} \times (\text{Lip09}) \times 16 \end{aligned} \quad (1)$$

with the ratios normalizing for the number of protons contributing to the signal. The last two terms in Eq. 1 include contributions for one carbonyl carbon (mass 12) and of two oxygen atoms (mass 16) per acid chain. The fLM is obtained as the mass ratio of the lipid mass divided by the sum of lipid plus water mass; hence

$$\text{fLM} = \frac{\text{lipid mass}}{\text{lipid mass} + \frac{1}{2} \cdot I_{\text{water}} \cdot 18} \quad (2)$$

I_{water} is the intensity of water signal, the factor 1/2 accounts for the 2 protons contributing to the water signal and 18 is molecular weight of water.

In ob/+ mice, the peak intensities of Lip41 and Lip43 were not included in the analysis due to interference of the residual water signal. Hence, fLM does not include the contribution of the carbon from these two structures, which lead to a slight underestimation of the lipid mass and fLM for ob/+ mice.

(b) We define the saturated lipid component (SL) as the averaged number of –CH_2– groups (Lip13) per fatty acid chain, which is obtained by normalization with Lip09 signal intensity as there is only one –CH_3 group per lipid chain. We used Lip09 instead of Lip16 or Lip23 for the quantification of number of chains, since the Lip09 resonance can be better separated from neighboring peaks leading to more reliable quantification results. Accordingly we obtain

$$\text{SL} = \frac{3}{2} \cdot \frac{\text{Lip13}}{\text{Lip09}}. \quad (3)$$

(c) The total unsaturated lipid component (UL_{total}) can be defined as the average number of carbon double bonds per fatty acid chain, i.e.

Table 1 Nine different peaks in proton magnetic resonance spectra obtained from liver assigned to different ^{1}H positions in lipids

Peak	Chemical shift (ppm)	Lipids-associated ^{1}H of the spectra
Lip09	0.90	**C**H_3–$(CH_2)_n$–
Lip13	1.30	–$(C$**H_2**$)_n$–
Lip16	1.60	–CH_2–O–CO–CH_2–**C**H_2–
Lip21	2.03	–CH_2–**C**H_2–CH=CH–
Lip23	2.25	–CH_2–O–CO–**C**H_2–CH_2–
Lip28	2.76	–CH=CH–**C**H_2–CH=CH–
Lip41	4.09	–**C**H_2–O–C(O)–CH_2–CH_2–
Lip43	4.28	–**C**H_2–O–C(O)–CH_2–CH_2–
Lip52&53	5.32	–**C**H**=C**H– and >**C**H–CH_2–O–C(O)–CH_2–CH_2–

$$UL_{total} = \frac{3}{2} \cdot \frac{Lip52\&53}{Lip09}. \quad (4)$$

The peak Lip52&53 contains contributions from both mono- and polyunsaturated lipids as well as the signal from glycerol [13], but our spectral resolution is not high enough to distinguish the various resonances. The relationship of Lip52&53 $-\frac{1}{9}$Lip09 was applied to exclude the contribution from glycerol in previous work by Giarola [36]. This is correct with the assumption that there is only triglyceride in hepatic lipids, which is not applicable for our study. The factor 2 in the denominator accounts for the fact that UL_{total} accounts for the number of double bonds and not the number of =CH– groups.

(d) The fraction of unsaturated lipids (fUL) is the average percentage of fatty acid chains with double carbon bond structure, including mono- and polyunsaturated fatty acids.

$$fUL = \frac{3}{4} \cdot \frac{Lip21}{Lip09} \quad (5)$$

The factor 1/4 accounts for the fact that adjacent to both single and double bonds there are two methylen groups with two protons each. The fraction of saturated lipids (fSL) is the percentage of fatty acid chain without carbon double bond, i.e.

$$fSL = 1 - fUL. \quad (6)$$

The fraction of polyunsaturated lipids (fPUL) is the percentage of fatty acid chains with multiple double bonds, i.e.

$$fPUL = \frac{3}{2} \cdot \frac{Lip28}{Lip09} \quad (7)$$

with the factor 1/2 accounting for the methylene group between two double bonds. The fraction of monounsaturated lipids (fMUL), i.e. the percentage of fatty acid chains comprising a single carbon double bond then becomes

$$fMUL = fUL - fPUL. \quad (8)$$

(e) The mean chain length (MCL) can be estimated as:

$$MCL = \frac{\frac{1}{3} \times Lip09 + \frac{1}{2} \times (Lip13 + Lip16 + Lip21 + Lip23 + Lip28) + Lip52\&53}{\frac{1}{3} \times Lip09} + 1, \quad (9)$$

where the term 1 accounts for one carbonyl group per chain.

Statistical analysis

All results are presented as mean ± SE. For statistical analysis OriginPro 8.1 (OriginLab, Northampton, MA, USA) was used. Data (ob/ob vs. ob/+) were analyzed using the one way ANOVA test. The level of significance was set as $\alpha = 0.05$.

Results

Cross-sectional MR images through the abdomen of ob/ob and ob/+ control mice reveal enlarged subcutaneous fat layers and enlarged liver volumes in ob/ob compared to the corresponding ob/+ control mice (Fig. 1). The localized in vivo MR spectroscopy of ob/ob and ob/+ mice at 9.4T typically showed nine lipid resonances, which were sufficiently resolved for quantification (Fig. 1) with the peak assignment given in Table 1.

The magnetic field homogeneity with a full width at half maximum of the water resonance of 58.1 ± 5.7 Hz and 50.9 ± 1.1 Hz for ob/ob and ob/+ control mice, respectively, was sufficient to clearly identify all of the nine lipid resonances. However, the large amount of accumulated fat in the liver of ob/ob mice affects local magnetic susceptibility, which may explain the slightly broader line width of the water peak.

Water suppression was not required for the analysis of lipid composition in the liver of ob/ob mice, since lipid signals were of comparable intensity as the water signal. In fact, water suppression was found, at least in part, to suppress the lipid resonances close to 4.65 ppm, resulting in a reduction of the intensity of peak Lip52&53 by 14% compared to the spectrum without water suppression. However, water suppression was required when studying ob/+ mice, since the relatively weak lipid resonances only became clearly distinguishable when suppressing the large water peak, which resulted in spectral distortions close to the water resonance frequency. For the sake of an accurate comparison of the quantitative results obtained for the two mouse lines tested, we have applied water suppression in all measurements. The LCModel could fit all nine different

lipid peaks accurately yielding CRLB lower than 20% for all peaks included.

The comparison of T_2 relaxation times for each lipid signal of ob/ob and ob/+ mice (Table 2) revealed some statistically significant differences. The T_2 value of water was found to be shorter in ob/ob compared to ob/+ mice (11.9 ± 1.0 ms vs. 14.3 ± 0.3 ms), while the T_2 value of Lip09 was significantly longer in ob/ob mice compared to ob/+ controls (42.1 ± 3.2 ms vs. 25.3 ± 2.8 ms). We did not observe any statistically significant differences in the T_2 values for any of the other lipid resonances. Because relaxation times T_2 were comparable to the T_E values used in the PRESS sequence, effects of differences in T_2 relaxation had to be accounted for in the quantitative analysis of the signals.

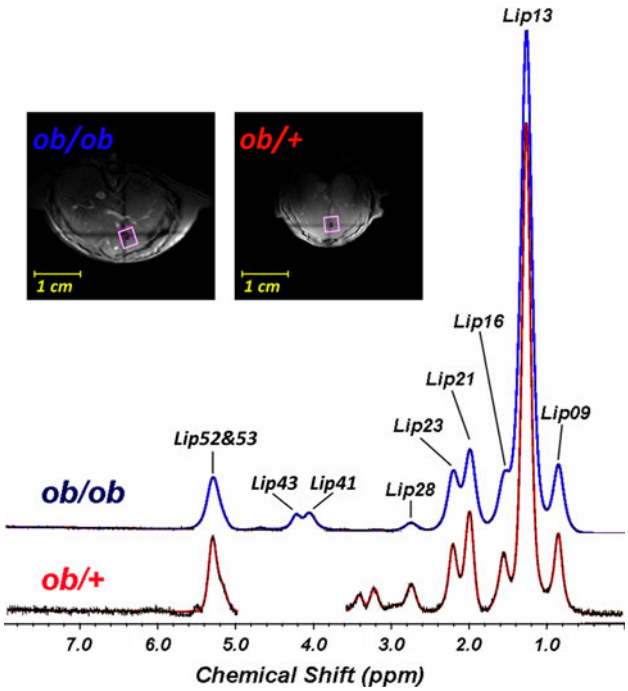

Fig. 1 Anatomical reference images with voxel for single voxel spectroscopy indicated (3 × 3 × 3 mm^3) and spectrum from ob/ob and ob/+ mice. Resonances are labeled according to their chemical shift values

The T_2 corrected signal intensities were scaled according to the number of protons contributing to each resonance peak. The peak intensities (the averaged intensity relative to the water signal is listed in Table 2) were used to derive values characterizing the lipid composition in the liver of the two different mouse groups (Table 3). As expected, the fractional lipid mass (fLM) differed significantly between ob/ob and ob/+ mice (0.217 ± 0.013 in ob/ob vs. 0.034 ± 0.010 in ob/+ mice, $P < 0.001$). A significant increase in the saturated lipid component (SL) of ob/ob mice could also be observed (9.85 ± 0.11 in ob/ob vs. 7.06 ± 0.41 in ob/+, $P < 0.001$), but not in the total unsaturated component (UL_{total}; $P = 0.12$). Similarly, no differences were found between ob/ob and ob/+ control mice in the fraction of unsaturated (fUL), the fraction of saturated (fSL) and the fraction of polyunsaturated (fPUL) lipids. However, the fraction of monounsaturated lipids (fMUL) with only one carbon–carbon double bond per chain was significantly higher in ob/ob mice compared to ob/+ mice. Correspondingly, the ratio of polyunsaturated to monounsaturated lipids was found significantly lower in ob/ob mice compared to ob/+ controls (0.40 ± 0.09 in ob/ob vs. 1.13 ± 0.34 in ob/+, $P = 0.026$). Furthermore, an increase in the mean chain length was observed in ob/ob mice compared to ob/+ mice (19.4 ± 0.4 in ob/ob vs. 15.8 ± 1.0 in ob/+, $P = 0.003$).

Discussion

^{1}H MR spectroscopic information on hepatic lipid composition can be obtained in multiple ways: by collecting

Table 2 Averaged T_2 values and relative intensity to water of individual lipids component and water in ob/ob and ob/+ control mice at 9.4*T*

Peak	T_2 values			Relative intensity to water		
	ob/ob	ob/+	*P*	ob/ob	ob/+	*P*
Lip09	42.1 ± 3.2	25.3 ± 2.8	**0.008**	2.32E−02 ± 2.09E−03	3.98E−03 ± 1.33E−03	1.21E−04
Lip13	42.5 ± 3.8	53.4 ± 4.2	0.076	1.52E−01 ± 1.23E−02	1.88E−02 ± 6.36E−03	3.03E−05
Lip16	15.6 ± 1.8	21.5 ± 13.0	0.497	2.26E−02 ± 1.26E−03	3.27E−03 ± 7.48E−04	1.91E−06
Lip21	33.7 ± 3.2	30.3 ± 3.9	0.508	2.73E−02 ± 1.37E−03	3.77E−03 ± 8.90E−04	8.08E−07
Lip23	27.4 ± 3.2	26.7 ± 8.7	0.931	1.80E−02 ± 1.22E−03	2.35E−03 ± 7.10E−04	8.31E−06
Lip28	25.0 ± 1.8	21.3 ± 2.9	0.275	3.64E−03 ± 4.80E−04	1.01E−03 ± 3.68E−04	5.00E−03
Lip52&53	37.8 ± 3.6	37.3 ± 2.0	0.948	2.14E−02 ± 1.84E−03	3.17E−03 ± 1.01E−03	6.03E−05
Water	11.9 ± 1.0	14.3 ± 0.3	**0.039**	1		
Lip41	16.5 ± 1.6			1.60E−02 ± 1.42E−03		
Lip43	14.0 ± 1.2			1.54E−02 ± 2.31E−03		

Shown are the mean and standard error

All the bold values are below 0.05, which means they are significant

Table 3 Hepatic lipid level and fat composition in ob/ob and ob/+ control mice

Parameter	ob/ob	ob/+	*P*
Fractional lipid mass (fLM)	0.217 ± 0.013	0.034 ± 0.010	**1.15E−06**
Saturated lipid component (SL)	9.854 ± 0.106	7.060 ± 0.408	**1.35E−05**
Total unsaturated component (UL_{total})	1.397 ± 0.063	1.210 ± 0.096	0.123
Fraction of unsaturated (fUL)	0.900 ± 0.038	0.770 ± 0.106	0.194
Fraction of saturated (fSL)	0.100 ± 0.038	0.230 ± 0.106	0.194
Fraction of polyunsaturated (fPUL)	0.248 ± 0.042	0.381 ± 0.085	0.146
Fraction of monounsaturated (fMUL)	0.652 ± 0.036	0.389 ± 0.072	**0.005**
fPUL/fMUL	0.398 ± 0.087	1.125 ± 0.340	**0.026**
Mean chain length (MCL)	19.4 ± 0.4	15.8 ± 1.0	**0.003**

Shown are the mean and standard error

All the bold values are below 0.05, which means they are significant

information from a single volume of interest (voxel), or in the form of low resolution images (chemical shift imaging or spectroscopic imaging) [21–24]. A disadvantage of the imaging procedures is long acquisition time and the higher complexity in deriving accurate quantification [23]. In contrast, single voxel MRS is rather straightforward, provides high spectral resolution, which is beneficial for deriving quantitative data. Its principal limitation is the local information provided, which may constitute an issue when sampling highly heterogeneous tissue.

Apart from signals of other metabolites, the liver ^{1}H PRESS spectra comprises contributions from mobile lipids including mono-, di- and triacylglycerols, non-esterified fatty acids, cholesterol, cholesterol ester [12, 20, 35]. Nine resonances arising from molecular constituents such as $–CH_3$, $–CH_2–$ and –CH– groups of the lipid chains can be typically resolved in the chemical shift range from 0.9 to 5.3 ppm (with the water reference at 4.65 ppm in LCModel). The intensities of these individual peaks can be used to extract detailed information on the composition of the lipids. Differences in biophysical parameters of chemical entities have to be accounted for when deriving quantitative data. The relaxation behavior of tissue (lipid and water) protons depends on their local chemical environment. Hence, different compounds/functional groups display different transverse and longitudinal relaxation times T_1 and T_2. T_1 effects can be accounted for by using a long repetition delay. Since we used $T_R = 6$ s with T_1 values of water at 9.4T being around 2 s [34] and T_1 of lipids even shorter (<1.2 s) [13, 18], we can assume that the lipid signals were almost fully recovered (>99% recovery), while there was some remaining saturation (approximately 95% recovery) for the water signal. This will lead to a slight (less than 5%) overestimation of the fractional lipid mass (fLM), which however is irrelevant in view of the changes between the two mouse strains. However, T_2 values of individual signals had to be considered in order to accurately determine even relative signal intensities [13, 18, 34].

In our analysis, we assumed that hepatic mobile lipids predominantly consist of saturated, mono- and polyunsaturated compounds. Moreover, we assumed that the distribution of lipids across the liver is homogeneous, as liver tissue appeared homogeneous in MR images. Previous reports confirmed a homogeneous distribution [37]. Nevertheless, we carefully positioned the PRESS voxel within the same anatomical location to ensure an accurate comparison of MRS data in different animals. In order to achieve good spectral quality, this location was chosen in a liver region at a fair distance to the organ margin and carefully avoiding contribution from major liver vessels. This minimized line broadening due to susceptibility changes across different tissues.

Changes in hepatic lipid composition reflect changes in whole body lipid metabolism [38]. It has been reported that ob/ob mice displayed higher levels of intracellular hepatic triglycerides as early as 2 weeks after birth [27, 28]. The level of fractional lipid mass (fLM) in ob/ob mice found in this study is in line with results obtained using conventional techniques [28]. fLM values in ob/+ controls were slightly higher than literature values though the difference was not significant (3.4 ± 1.0% vs. 2.7% estimated from literature [28] assuming a mean molecular weight of triglycerides of 800 Dalton). An important finding was a significantly longer mean chain length in ob/ob as compared to ob/+ mice. In ob/ob mice, influx of free fatty acid from circulation is increased [39]. Moreover, fatty acid synthesis activity, de novo hepatic long chain fatty acid and triglyceride synthesis are elevated, however the very low density lipoprotein synthesis and TG export are not increased [3, 28, 40]. In combination with impaired liver mitochondrial β-oxidation, hepatic lipids accumulate, in particular the long chain fatty acyl-CoA [27, 31]. This might contribute to longer mean chain length of hepatic lipid in ob/ob mice as compared to ob/+ controls.

We also observed that the saturated lipid components (SL) and fraction of monounsaturated lipids (fMUL) are significantly higher in ob/ob mice compared to ob/+ controls. In contrast, the total unsaturated component (UL_{total}), the fraction of saturated (fSL) and unsaturated lipids (fUL), as well as the fraction of polyunsaturated lipids (fPUL)

were not different between these two groups. Nevertheless, taken into account the higher amount of lipids of ob/ob mice, the concentration of unsaturated hepatic lipid is higher in ob/ob than ob/+ control mice, which might be more relevant with regard to liver function than the actual composition. The ratio of polyunsaturated to monounsaturated lipids is significantly lower in ob/ob mice than in ob/+ controls, which might indicate depletion of polyunsaturated fatty acid in obesity-related hepatic steatosis [38].

The determination of lipid levels and composition from ^{1}H MRS spectra raises several issues that may affect quantification inherently:

1. Limited spectral resolution may lead to contamination of individual lipid resonances by signal contributions from other metabolites, which will affect the intensity measurement [8, 11, 20].
2. Spectral dispersion translates into chemical shift displacement, an intrinsic property of a gradient based localization technique such as PRESS. Proportional to the chemical shift value of a given resonance, the selected voxel will be shifted in all three dimensions. Hence the individual resonances are not measured exactly at the same position. For the gradient strength used in our experiments, the chemical shift displacement between the voxel corresponding to water peak and that of the Lip13 peak amounts to approximately 0.8 mm (for a voxel dimension of 3 mm). This might be a potential source of error, but should not be critical for our analysis, since we assume a homogeneous lipid composition in the liver.
3. The result of the spectral analysis will depend on the accuracy of the theoretical lineshape model applied. In this study, we have applied LCModel using Lorentzian–Gaussian lineshapes. The in vivo signals are the sum of ^{1}H spin-coupled multiplets from several different fatty acids with slightly different chemical shifts that cannot be resolved [20]. Consequently, a single Lorentzian–Gaussian line will not properly represent the experimental lineshape, which might translate into small errors in quantification [41].
4. As already mentioned, T_2 relaxation has to be adapted to obtain comparable intensity readouts. The signals observed in our experiments are the superposition of multiple resonances, and therefore a single exponential model may not be accurate. Our experimental data are not sufficient to allow multi-exponential regression analysis, as this would be a better way to perform the analysis.
5. Due to J-coupling T_2 values obtained from PRESS experiments are smaller than those obtained when using the STEAM sequence [42, 43], which might affect the accuracy of the intensity quantification. Based on literature data [43], we estimated that the effect of J-coupling modulation on $I(0)$ values would be of the order of $\pm 10\%$, which would translate into corresponding uncertainties regarding the parameters describing the lipid composition The conclusion regarding these parameters describing hepatic lipid composition is not affected by the deviation. Statistically significant differences between ob/ob and ob/+ mice would still be found for the parameters fLM, SL, fMUL and fPUL/fMUL. Only for the MCL, the difference might become non-significant in the most unfavourable case.

Some of the above mentioned drawbacks of the ^{1}H MRS measurements might be addressed by using proton-decoupled ^{13}C MRS. This approach yields a significantly higher spectral dispersion and therefore allows a more detailed characterization of the fat composition [8, 14]. In fact, there are reports demonstrating consistent results between ^{13}C MRS derived lipid concentrations and values obtained from lipid extraction followed by chromatographic analysis [8]. Yet, clinical translation of such an approach is challenging: natural abundance ^{13}C MRS suffers from low sensitivity and correspondingly from low spatial resolution. In addition, the large chemical shift range in ^{13}C spectra will lead to substantial chemical shift displacements. Both limitations can be addressed using ^{1}H–^{13}C polarization transfer techniques, which are technically challenging and face other limitations [37, 38]. Moreover, ^{13}C MRS requires a two channel system, whereas ^{1}H MRS experiments can be carried out in principle on any clinical scanner.

The potential of the ^{1}H MRS approach might be further enhanced by chemical shift imaging/spectroscopic imaging. This provides spatially resolved information on the hepatic lipid distribution in two or even three dimensions, and complements the data on lipid composition with spatial information [23].

^{1}H MRS has emerged as attractive tool to assess lipid metabolism in vivo noninvasively in mice in various tissue compartments such as adipose tissue [18], skeletal muscle [44] and liver under normal and pathological conditions. Due to cross-talk between adipose tissues and liver, it's interesting to evaluate the lipid content and composition in adipose tissues for further study. Combining these readouts and monitoring tissue specific lipid accumulation and composition in a longitudinal manner in mouse models of metabolic disorders (including genetically engineered mice) might provide novel insights into mechanistic aspects underlying the pathogenesis of hepatic steatosis.

Conclusion

In conclusion, we applied ^{1}H MRS measurements at 9.4T to assess the amount of hepatic lipids as well as the fat

composition in ob/ob and ob/+ control mice in vivo and non-invasively from a voxel of $3 \times 3 \times 3$ mm^3. Significant differences between these two lines have been found for the fractional lipid mass (fLM), saturated lipid component (SL) as well as the fraction of monounsaturated lipids (fMUL). Moreover, the mean chain length (MCL) and the ratio of polyunsaturated to monounsaturated lipids (fPUL/fMUL) differ significantly. These changes reflect alterations in the general lipid metabolism of the mice, which is attractive given the large number of genetically engineered mouse line available for mechanistic studies.

Acknowledgments We gratefully acknowledge funding by the Swiss National Science Foundation and SystemsX.ch. We also thank René Tschaggelar and Nikola Cesarovic for excellent technical assistance during various aspects of this study. We especially thank Prof. Peter Boesiger for providing kind access to LCModel and Dr. Anke Henning for advice.

References

1. Krssak M, Roden M (2004) The role of lipid accumulation in liver and muscle for insulin resistance and type 2 diabetes mellitus in humans. Rev Endocr Metab Disord 5:127–134
2. Kovacs P, Stumvoll M (2005) Fatty acids and insulin resistance in muscle and liver. Best Pract Res Clin Endocrinol Metab 19: 625–635
3. Anstee QM, Goldin RD (2006) Mouse models in non-alcoholic fatty liver disease and steatohepatitis research. Int J Exp Pathol 87:1–16
4. Craske JD (1993) Separation of instrumental and chemical errors in the analysis of oils by gas-chromatography—a collaborative evaluation. J Am Oil Chem Soc 70:325–334
5. Deman JM (1964) Determination of fatty acid composition of milk fat by dual column temperature programmed gas-liquid chromatography. J Dairy Sci 47:546–547
6. Lindon JC, Holmes E, Nicholson JK (2006) Metabonomics techniques and applications to pharmaceutical research and development. Pharm Res 23:1075–1088
7. Zancanaro C, Nano R, Marchioro C et al (1994) Magnetic resonance spectroscopy investigations of brown adipose tissue and isolated brown adipocytes. J Lipid Res 35:2191–2199
8. Knothe G, Kenar JA (2004) Determination of the fatty acid profile by H-1-NMR spectroscopy. Eur J Lipid Sci Tech 106:88–96
9. Miyake Y, Yokomizo K, Matsuzaki N (1998) Determination of unsaturated fatty acid composition by high-resolution nuclear magnetic resonance spectroscopy. J Am Oil Chem Soc 75:1091–1094
10. Yeung DKW, Lam SL, Griffith JF et al (2008) Analysis of bone marrow fatty acid composition using high-resolution proton NMR spectroscopy. Chem Phys Lipids 151:103–109
11. Guillen MD, Ruiz A (2003) H-1 nuclear magnetic resonance as a fast tool for determining the composition of acyl chains in acylglycerol mixtures. Eur J Lipid Sci Tech 105:502–507
12. Ruberg FL, Viereck J, Phinikaridou A et al (2006) Identification of cholesteryl esters in human carotid atherosclerosis by ex vivo image-guided proton MRS. J Lipid Res 47:310–317
13. Ren JM, Dimitrov I, Sherry AD et al (2008) Composition of adipose tissue and marrow fat in humans by H-1 NMR at 7 Tesla. J Lipid Res 49:2055–2062
14. Hwang JH, Bluml S, Leaf A et al (2003) In vivo characterization of fatty acids in human adipose tissue using natural abundance H-1 clecoupled C-13 MRS at 1.5 T: clinical applications to dietary therapy. NMR Biomed 16:160–167
15. Lunati E, Farace P, Nicolato E et al (2001) Polyunsaturated fatty acids mapping by (1)H MR-chemical shift imaging. Magn Reson Med 46:879–883
16. Walling BE, Munasinghe J, Berrigan D et al (2007) Intra-abdominal fat burden discriminated in vivo using proton magnetic resonance spectroscopy. Obesity (Silver Spring) 15:69–77
17. Lunati E, Marzola P, Nicolato E et al (1999) In vivo quantitative lipidic map of brown adipose tissue by chemical shift imaging at 4.7 tesla. J Lipid Res 40:1395–1400
18. Strobel K, van den Hoff J, Pietzsch J (2008) Localized proton magnetic resonance spectroscopy of lipids in adipose tissue at high spatial resolution in mice in vivo. J Lipid Res 49:473–480
19. Lundbom J, Hakkarainen A, Soderlund S et al (2011) Long-TE (1)H MRS suggests that liver fat is more saturated than subcutaneous and visceral fat. NMR Biomed 24:238–245
20. Bollard ME, Garrod S, Holmes E et al (2000) High-resolution (1)H and (1)H–(13)C magic angle spinning NMR spectroscopy of rat liver. Magn Reson Med 44:201–207
21. Corbin IR, Furth EE, Pickup S et al (2009) In vivo assessment of hepatic triglycerides in murine non-alcoholic fatty liver disease using magnetic resonance spectroscopy. Bba-Mol Cell Biol L 1791:757–763
22. Calderan L, Marzola P, Nicolato E et al (2006) In vivo phenotyping of the ob/ob mouse by magnetic resonance imaging and 1H-magnetic resonance spectroscopy. Obesity (Silver Spring) 14:405–414
23. Griffitts J, Tesiram Y, Reid GE et al (2009) In vivo MRS assessment of altered fatty acyl unsaturation in liver tumor formation of a TGF alpha/c-myc transgenic mouse model. J Lipid Res 50:611–622
24. Garbow JR, Lin X, Sakata N et al (2004) In vivo MRS measurement of liver lipid levels in mice. J Lipid Res 45:1364–1371
25. Dimitrov IE, Douglas D, Ren J et al (2011) In vivo determination of human breast fat composition by (1) H magnetic resonance spectroscopy at 7 T. Magn Reson Med 67:20–26
26. Mosconi E, Fontanella M, Sima DM et al (2011) Investigation of adipose tissues in Zucker rats using in vivo and ex vivo magnetic resonance spectroscopy. J Lipid Res 52:330–336
27. Lindstrom P (2007) The physiology of obese-hyperglycemic mice [ob/ob mice]. Sci World J 7:666–685
28. Menahan LA (1983) Age-related changes in lipid and carbohydrate metabolism of the genetically obese mouse. Metabolism 32:172–178
29. Cheng Y, Zhang J, Shang J et al (2009) Prevention of free fatty acid-induced hepatic lipotoxicity in HepG2 cells by magnesium isoglycyrrhizinate in vitro. Pharmacology 84:183–190
30. Duncan JG (2008) Lipotoxicity: what is the fate of fatty acids? J Lipid Res 49:1375–1376
31. Choo HJ, Kim JH, Kwon OB et al (2006) Mitochondria are impaired in the adipocytes of type 2 diabetic mice. Diabetologia 49:784–791
32. Chance DS, Mcintosh MK (1994) Rates of beta-oxidation of fatty-acids of various chain lengths and degrees of unsaturation in highly purified peroxisomes isolated from rat-liver. Comp Biochem Phys B 109:273–280
33. Shimano H, Matsuzaka T, Yahagi N et al (2007) Crucial role of a long-chain fatty acid elongase, Elovl6, in obesity-induced insulin resistance. Nat Med 13:1193–1202
34. de Graaf RA, Brown PB, McIntyre S et al (2006) High magnetic field water and metabolite proton T-1 and T-2 relaxation in rat brain in vivo. Magn Reson Med 56:386–394

35. Delikatny EJ, Chawla S, Leung DJ et al (2011) MR-visible lipids and the tumor microenvironment. NMR Biomed 24:592–611
36. Giarola M, Rossi B, Mosconi E et al (2011) Fast and minimally invasive determination of the unsaturation index of white fat depots by micro-raman spectroscopy. Lipids 46:659–667
37. Machann J, Thamer C, Schnoedt B et al (2006) Hepatic lipid accumulation in healthy subjects: a comparative study using spectral fat-selective MRI and volume-localized H-1-MR spectroscopy. Magn Reson Med 55:913–917
38. Johnson NA, Walton DW, Sachinwalla T et al (2008) Noninvasive assessment of hepatic lipid composition: advancing understanding and management of fatty liver disorders. Hepatology 47:1513–1523
39. Yki-Jarvinen H (2005) Fat in the liver and insulin resistance. Ann Med 37:347–356
40. Li X, Grundy SM, Patel SB (1997) Obesity in db and ob animals leads to impaired hepatic very low density lipoprotein secretion and differential secretion of apolipoprotein B-48 and B-100. J Lipid Res 38:1277–1288
41. Dong Z, Dreher W, Leibfritz D et al (2009) Challenges of using MR spectroscopy to detect neural progenitor cells in vivo. Am J Neuroradiol 30:1096–1101
42. Yahya A, Fallone BG (2010) T(2) determination of the J-coupled methyl protons of lipids: in vivo illustration with tibial bone marrow at 3 T. J Magn Reson Imaging 31:1514–1521
43. Yahya A, Tessier AG, Fallone BG (2011) Effect of J-coupling on lipid composition determination with localized proton magnetic resonance spectroscopy at 9.4 T. J Magn Reson Imaging 34: 1388–1396
44. Ye Q, Danzer CF, Fuchs A et al (2011) Longitudinal evaluation of intramyocellular lipids (IMCLs) in tibialis anterior muscle of ob/ob and ob/+ control mice using a cryogenic surface coil at 9.4 T. NMR Biomed 24:1295–1301